Journal of Cerebral Blood Flow & Metabolism (2011) 31, 1211–1222
© 2011 ISCBFM All rights reserved 0271-678X/11 $32.00
www.jcbfm.com

Temporal dynamics and spatial specificity of arterial and venous blood volume changes during visual stimulation: implication for BOLD quantification

Tae Kim[1] and Seong-Gi Kim[1,2]

[1]*Department of Radiology, University of Pittsburgh, Pittsburgh, Pennsylvania, USA;*
[2]*Department of Neurobiology, University of Pittsburgh, Pittsburgh, Pennsylvania, USA*

Determination of compartment-specific cerebral blood volume (*CBV*) changes is important for understanding neurovascular physiology and quantifying blood oxygenation level-dependent (BOLD) functional magnetic resonance imaging (fMRI). In isoflurane-anesthetized cats, we measured the spatiotemporal responses of arterial *CBV* (CBV_a) and total *CBV* (CBV_t) induced by a 40-second visual stimulation, using magnetization transfer (MT)-varied BOLD and contrast-agent fMRI techniques at 9.4 T. To determine the venous *CBV* (CBV_v) change, we calculated the difference between CBV_t and CBV_a changes. The dynamic response of CBV_a was an order of magnitude faster than that of CBV_v, while the magnitude of change under steady-state conditions was similar between the two. Following stimulation offset, ΔCBV_a showed small poststimulus undershoots, while ΔCBV_v slowly returned to baseline. The largest CBV_a and CBV_t response occurred after 10 seconds of simulation in cortical layer 4, which we identified as the stripe of Gennari by T_1-weighted MRI. The CBV_v response, however, was not specific across the cortical layers during the entire stimulation period. Our data indicate that rapid, more-specific arterial vasodilation is followed by slow, less-specific venous dilation. Our finding implies that the contribution of CBV_v changes to BOLD signals is significant for long, but not short, stimulation periods.
Journal of Cerebral Blood Flow & Metabolism (2011) **31,** 1211–1222; doi:10.1038/jcbfm.2010.226; published online 22 December 2010

Keywords: BOLD; *CBV*; $CMRO_2$; cortical layer; stripe of Gennari; visual cortex

Introduction

Functional magnetic resonance imaging (fMRI) techniques allow for noninvasive visualization of hemodynamic responses induced by neural activities. However, it remains controversial as to whether the area of changes in the fMRI signal fully corresponds with the site of increased neural activity, and whether the most commonly used blood oxygenation level-dependent (BOLD) fMRI signals can be quantified as physiological parameters. The laminar structure of the visual cortex has been used for examination of the spatial localization of fMRI signals (Goense and Logothetis, 2006; Harel *et al*, 2006; Jin and Kim, 2008*a*; Kim and Kim, 2010; Logothetis *et al*, 2002; Walters *et al*, 2003; Zhao *et al*, 2006). The middle of the cortex (layer 4) has the highest capillary density and metabolic responses in the primary sensory cortical areas (Payne and Peters, 2002; Woolsey *et al*, 1996). In humans and nonhuman primates, layer 4 contains the myelin-rich stripe of Gennari in the primary visual cortex and is identified by its prominent anatomical MRI contrast (Barbier *et al*, 2002; Logothetis *et al*, 2002; Walters *et al*, 2003). Although the laminar model in the cat visual cortex has been used (Harel *et al*, 2006; Jin and Kim, 2008*a*; Kim and Kim, 2010; Zhao *et al*, 2006), the location of layer 4 in anatomical MR images remains undetermined. As brain topography varies among individual cats, it is extremely advantageous to know the *in vivo* MRI correlation between the structural and functional contrast of cortical layers.

In cortical layer-dependent functional studies with large activation areas, the largest change in conventional gradient-echo BOLD fMRI signals occurs at the cortical surface, but the largest change in cerebral blood volume (*CBV*) responses appears in the middle

Correspondence: Dr T Kim, Department of Radiology, University of Pittsburgh, 3025 East Carson Street, Pittsburgh, PA 15203, USA.
E-mail: tak19@pitt.edu
This work was supported by NIH grants EB003324, EB003375, and NS44589, and was presented in part at the 17th Annual Meeting of the International Society for Magnetic Resonance in Medicine.
Received 21 July 2010; revised 29 October 2010; accepted 30 November 2010; published online 22 December 2010

of the cortex (Harel *et al*, 2006; Jin and Kim, 2008*a*; Lu *et al*, 2004; Mandeville and Marota, 1999; Zhao *et al*, 2006). Unlike increased venous oxygenation, an increase in venous *CBV* decreases BOLD fMRI signals. Thus, it is important to separate total *CBV* (CBV_t) into arterial and venous *CBV* (CBV_a and CBV_v, respectively) changes to quantify BOLD fMRI signals as physiological parameters, and to better understand compartment-specific vascular responses. Here, we define CBV_a as the blood volume within arterial vessels of all sizes, including a portion of capillaries, and CBV_v as the remainder of CBV_t; thus, if CBV_t and CBV_a are known, we can calculate CBV_v. We can determine the CBV_a change using our newly developed magnetization transfer (MT)-varied fMRI technique (Kim *et al*, 2008; Kim and Kim, 2010). When a long off-resonance radio frequency (RF) pulse is applied, MT effects reduce tissue water signals and could produce a similar effect on venous blood due to the upstream free exchange between tissue water and capillary water. In contrast, the arterial blood pool experiences only a minimal MT effect as there is an inflow of fresh blood spins unaffected by the MT-inducing pulse. Thus, MT-insensitive arterial blood signals can be separated from MT-dependent extravascular tissue and venous blood.

Based on our previous 15 seconds somatosensory stimulation studies in isoflurane-anesthetized rats, the CBV_a change is dominant while the CBV_v change is negligible (Kim *et al*, 2007). In two separate fMRI studies in isoflurane-anesthetized cats, time-dependent spatial responses of CBV_t and CBV_a across the visual cortex appear similar (Jin and Kim, 2008*a*) and (Kim and Kim, 2010), suggesting that CBV_t changes originate mostly from arterial vessels, the responses share a similar special specificity, or both. However, CBV_a and CBV_v compartments may undergo different dynamic changes during neural stimulation; thus, responses may depend upon the duration of stimulation. Indeed, CBV_t-weighted fMRI signals in the rat somatosensory cortex occur as two components: an early rapid response followed by a slow prolonged response (Mandeville *et al*, 1999; Silva *et al*, 2007). Important questions include whether the slow CBV_t response originates from passively responding venous vessels, and whether the spatial specificity of CBV_v is similar to that of CBV_a. Systemic examination of functional CBV_a versus CBV_v responses will determine whether our previous finding of the dominant CBV_a change resulted from relatively short stimulus duration (15 seconds); how the spatial specificity of *CBV* responses varies with the stimulus duration; and when the CBV_v response is significant.

In this study, each cat was used to both identify layer 4 in the visual cortex by imaging the stripe of Gennari with T_1-weighted images, and measure functional CBV_a and CBV_t changes (ΔCBV_a and ΔCBV_t) during 40 seconds visual stimulation by MT-varied BOLD and contrast-agent fMRI techniques. We used the difference in ΔCBV_a and ΔCBV_t time courses to determine the dynamic change in CBV_v (ΔCBV_v). Temporal characteristics of ΔCBV_a and ΔCBV_v were compared to identify the sources of early and late contributions to CBV_t responses. To investigate time-dependent spatial specificity, we obtained functional maps and cortical profiles of ΔCBV_a, ΔCBV_t and ΔCBV_v during four 10-second stimulation periods, and compared these with *in vivo* high-resolution anatomical images to correlate structure and function.

Materials and methods

Animal Preparation and Visual Stimulation

Nine adolescent cats weighing 1.1 to 2.0 kg were performed with the approval from the University of Pittsburgh Institutional Animal Care and Use Committee: two cats for visualization of anatomic cortical structure with *in vivo* and *fixed brain* MRI, and seven cats for fMRI studies. The animals were anesthetized with 1.0% to 1.1% isoflurane with air supplemented with O_2 to attain a total O_2 level of $\sim$30%. End-tidal CO_2 was maintained in the range of 3.5% to 3.8%. Rectal temperature was maintained at 38.5°C ± 0.5 °C. For visual stimulation, binocular, full-field, black (0.5 cd/cm^2) and white (29 cd/cm^2) square-wave moving gratings (spatial frequency: 0.15 cycles/degree, temporal frequency: 2 cycles/s) were presented. It is noted that much higher luminance was used for our laboratory's previous visual stimulation studies (Jin and Kim, 2008*a*, *b*; Zhao *et al*, 2006). The details of animal preparation and visual stimulation were described previously (Kim and Kim, 2010).

Overall Magnetic Resonance Imaging Acquisitions

All MRI measurements were performed using a 9.4T/31-cm magnet interfaced to a Unity INOVA console (Varian, Palo Alto, CA, USA) and an actively shielded 12 cm gradient coil, with a maximal strength of 400 mT/m and rise time of 130 microseconds. A 1.5-cm diameter surface coil was used. Magnetic field homogeneity was manually optimized using a slab, twice the imaging-slice thickness.

Visualization of Anatomical Structure in the Primary Visual Cortex

A coronal slice of a T_1-weighted image was acquired using a four-segmented turbo-fast low angle shot (FLASH) technique with pixel resolution = 78 μm × 78 μm × 2 mm, field of view = 2.0 × 2.0 cm^2, flip angle = $\sim$10°, echo time (*TE*) = 5 milliseconds, repetition time (*TR*) = 10 milliseconds, intersegment delay = 4 seconds, and an inversion time (TI) of 1.2 and 1.4 seconds. Total *CBV*-weighted maps ($\Delta R^*_{2,\mathrm{MION}}$) were also measured by FLASH images (without inversion) before and after a bolus injection of $\sim$12 mg Fe/kg dextran-coated monocrystalline iron oxide nanoparticles (MIONs). The images were acquired with *TR* = 40 milliseconds, *TE* = 10 to 15 milliseconds, intersegment delay = 100 milliseconds, and the same pixel size as T_1-weighted images. After the MR experiments, cat brains were fixed with 4% paraformaldehyde in 0.1 mol/L phosphate-

buffered saline ($n = 2$), and then placed in a container with agarose gel for MRI. As the fixation changes T_1 values of the brain, the TI value was adjusted to 850 milliseconds to replicate the cortical contrast of the *in vivo* images. Following the MR scan, a 4-mm coronal slab was extracted from the fixed brain ($n = 1$). We stained ten 10-μm thick slices with Luxol Fast Blue/Cresyl Violet to visualize myelin and Nissl bodies. The histological cortical profile was compared with the corresponding T_1-weighted image.

Functional Magnetic Resonance Imaging Studies: ΔCBV_a and ΔCBV_t

Preliminary multislice gradient-echo BOLD fMRI was performed in the visual cortical area. We then selected one 2-mm thick coronal slice for fMRI studies from each cat. High-resolution T_1-weighted anatomical images (field of view = $2.0 \times 2.0\,cm^2$, matrix size = 128×128) were obtained from the same slice to identify brain structures by the two-segmented turbo-FLASH technique with a TI of 1.4 seconds. Functional magnetic resonance imaging data were obtained using a single-shot EPI technique with in-plane resolution = $312\,\mu m \times 312\,\mu m$, flip angle = 20° to 30°, and *TR* of 1 second. Each fMRI run consisted of 50 prestimulation, 40 stimulation and 100 poststimulation images, repeated $\sim$20 times for signal averaging.

Measurement of Functional ΔCBV_a

Stimulus-induced ΔCBV_a measurements were performed with *TR* = 1 second (880 milliseconds off-resonance MT pulse duration with 5,000 Hz offset to water, 20 milliseconds delay, and 100 milliseconds slice excitation and data acquisition), and *TE* = 20 milliseconds. The RF power level of MT-inducing pulses was adjusted to achieve intensities of visual cortical area ($S_{ss,MT}$) to 1, $\sim$0.7 and $\sim$0.4 ($n = 4$), or 1 and $\sim$0.4 ($n = 3$) of the steady-state signal without MT effects. Details of theoretical background and methods were described previously (Kim *et al*, 2008; Kim and Kim, 2010).

Measurement of Functional ΔCBV_t

Stimulus-induced CBV_t changes were measured with the same parameters as ΔCBV_a measurements, except without MT pulses and a *TE* of 13 milliseconds after the intravenous administration of 7 to 15 mg Fe/kg MION. For the calculation of ΔR_2^* induced by MION without stimulation ($\Delta R^*_{2,MION}$), images were separately measured with *TE* = 20 milliseconds before each fMRI run.

Data Processing

General data processing: Data analysis was performed with STIMULATE, ImageJ, and in-house Matlab routines (Mathworks, Natick, MA, USA). For each study, all runs with identical conditions were averaged to generate group data. The first 10 seconds of prestimulation data was excluded to ensure that the steady-state condition was met. The baseline images included data acquired 40 seconds before simulation, while the stimulation images included data acquired between 1 and 40 seconds after stimulation onset. Individual results were averaged and group data are reported as mean ± s.d.

Calculation of CBV_a, CBV_t, and CBV_v Changes

For ΔCBV_a calculations, stimulus-induced changes ($\Delta S_{ss,MT}$) at each MT level was normalized to the fully relaxed signal S_0 ($\Delta S_{ss,MT}/S_0$). Then, these normalized signal changes were linearly fit against corresponding normalized baseline signals at each MT level ($S_{ss,MT}/S_0$). ΔCBV_a (units of mL blood/g tissue) values were obtained by multiplying the intercept with a tissue-to-blood partition coefficient of 0.9 mL/g (Herscovitch and Raichle, 1985).

The susceptibility-induced change in R_2^* by MION injection ($\Delta R^*_{2,MION}$) was linearly related to the CBV_t value in the baseline condition: $\Delta R^*_{2,MION} = \kappa \times CBV_t$, where κ is a constant dependent on the concentration of MION in blood (Kennan *et al*, 1998). Determination of an accurate κ requires a susceptibility change of the blood, but in our survival experiments, we could not withdraw the large amount of blood needed, and thus did not quantify κ as previously (Kim *et al*, 2007). Instead, $\Delta R^*_{2,MION}$ was calculated by $\ln(S_{pre}/S_{post})/TE$, where S_{pre} and S_{post} are signal intensities with a *TE* of 20 milliseconds before and after the MION injection, respectively. The stimulus-induced relaxation rate change after MION injection is also linearly related to the absolute ΔCBV_t. As the magnitude of the negative CBV_t-weighted fMRI response ($\Delta R^*_{2,stim,MION}$) after the MION injection is reduced by the positive BOLD response ($\Delta R^*_{2,stim}$), the BOLD signal must be removed from the CBV_t-weighted fMRI response (Kennan *et al*, 1998); $\Delta R^*_{2,stim,MION} - \Delta R^*_{2,stim}$ ($= \kappa \times \Delta CBV_t$), where ΔR_2^* is computed by $-\ln(S_{stim}/S_{base})/TE$, where S_{base} and S_{stim} are the signals under baseline and stimulation conditions, respectively. Note that the BOLD signal should be obtained from fMRI data without MT effects. Relative CBV_t change ($\Delta CBV_t/CBV_t$) was calculated as $(\Delta R^*_{2,stim,MION} - \Delta R^*_{2,stim})/\Delta R^*_{2,MION}$ (i.e., $\kappa \times \Delta CBV_t / \kappa \times CBV_t$).

To compare ΔCBV_a, ΔCBV_t, and ΔCBV_v, we converted $\Delta CBV_t/CBV_t$ to ΔCBV_t by estimating baseline CBV_t. In the intracortical region of interest (ROI) covering the most active pixels, three different baseline CBV_t values were assumed to cover an adequate CBV_t range: (1) $CBV_t = \Delta CBV_a/(\Delta CBV_t/CBV_t)$, assuming the peak amplitude of ΔCBV_t = the peak amplitude of ΔCBV_a (Kim *et al*, 2007); (2) a fixed value of 4.5 mL/100 g; and (3) a fixed value of 5.0 mL/100 g. The assumption of the ΔCBV_t peak = the ΔCBV_a peak defines the lower limit of the CBV_t value. The constant κ was determined by $\kappa = CBV_t/\Delta R^*_{2,MION}$ in the intracortical ROI. Time-dependent ΔCBV_t was calculated by $(\Delta R^*_{2,stim,MION} - \Delta R^*_{2,stim})/\kappa$. ΔCBV_v was obtained from the subtraction of ΔCBV_a from ΔCBV_t. As three baseline CBV_t values were assumed, three corresponding ΔCBV_t and ΔCBV_v values were determined.

Generation of Functional Cerebral Blood Volume Maps

All images were smoothed with a 2D Gaussian filter (kernel size = 3×3, sigma = 0.5). ΔCBV_a and $\Delta CBV_t/CBV_t$ and ΔCBV_v maps were generated for the entire 40 seconds

stimulation period. In addition, the stimulation period was divided into four equal parts and maps generated for each: 1 to 10 seconds, 11 to 20 seconds, 21 to 30 seconds, and 31 to 40 seconds.

Images from the baseline and the stimulation conditions were averaged for each MT level. To calculate ΔCBV_a maps, only activated pixels satisfying a P value <0.05 (for baseline versus stimulation conditions) at all MT levels were selected. ΔCBV_a was then obtained on a pixel-by-pixel basis, excluding the pixels with negative intercepts due to the contamination of cerebrospinal fluid (CSF) signals (Kim and Kim, 2010). For $\Delta CBV_t/CBV_t$ maps, only pixels with a P value <0.05 in both *CBV*-weighted fMRI and BOLD fMRI without MT were selected. ΔCBV_t maps were generated by pixel-wise calculation assuming the peak ΔCBV_t = peak ΔCBV_a for the lowest ΔCBV_t, and $CBV_t = 5$ mL/100 g for the highest ΔCBV_t. ΔCBV_v was then calculated by subtracting ΔCBV_a from ΔCBV_t, but only for positively activated pixels in both ΔCBV_a and ΔCBV_t maps.

Hemodynamic Responses of Cerebral Blood Volume Changes

Temporal dynamics were determined on a ROI basis without applying the spatial filter. We chose the following four ROIs: (1) an entire intracortical ROI covering the primary visual cortex; (2) a middle cortical ROI based on anatomical T_1-weighted MRI contrast; (3) an upper cortical ROI; and (4) a lower cortical ROI. The middle, upper, and lower cortical ROIs had the same sum as the entire intracortical ROI. Signals from all pixels within the ROI were averaged to obtain fMRI time courses. ΔCBV_t, ΔCBV_a, and ΔCBV_v time courses were then calculated. These time courses were fit with a single-exponential hemodynamic response function convolved with the boxcar stimulus function; time-constant and steady-state amplitudes were obtained. As ΔCBV_v time courses have low sensitivity, only averaged time courses across all seven animals were used for fitting.

Time-Dependent Cortical Depth Profiles of Cerebral Blood Volume Changes

We performed cortical depth profile analysis in area 18 within the visual cortex, as described previously (Zhao *et al*, 2006). Images were spatially interpolated using a bilinear method to match the resolution of the T_1-weighted anatomical images without smoothing. To generate a signal profile in the cortical depth dimension, we selected two quadrangular ROIs (one within each hemisphere) from the cortex surface to the gray/white-matter boundary, based on T_1-weighted anatomical images in each animal (Figure 5A), except for one animal in which the cortical surface in one hemisphere was distorted by large draining vein artifacts. The cortical depth was spatially interpolated to 11 pixels from the cortical surface to the white matter, resulting in an average depth resolution of 163 μm. The signals at the same relative cortical depths were averaged. Depth-dependent ΔCBV_t, ΔCBV_a, and ΔCBV_v values were then determined for each 10-second time period following the onset of stimulation, and their cortical profiles plotted as the distance from the cortical surface. The profiles of T_1-weighted images were also obtained for an anatomical reference of layer 4. Cortical layer locations were approximately assigned based on relative distances of those layers in area 18 (Payne and Peters, 2002).

Results

Visualization of Anatomical Structure in the Primary Visual Cortex

Hyperintense layers were clearly visible in the middle cortical regions (outlined by dashed lines) in T_1-weighted images with TI = 1.4 seconds (Figure 1A). However, with TI = 1.2 seconds, these layers became hypointense (data not shown), indicating that the signal source of these stripes is related to longitudinal relaxation properties. The source of this contrast is derived from the myelin-rich stripe of Gennari, a prominent feature in layer 4. The baseline CBV_t-weighted ($\Delta R^*_{2,\mathrm{MION}}$) map (Figure 1B) shows higher CBV_t values at the surface and the middle cortical layers, and at penetrating vessels (arrows). The high CBV_t values in the middle cortical layers is consistent with the high vascular density found in layer 4 (Tieman *et al*, 2004). This area also colocalized with the hyperintense stripes in the T_1-weighted images (see dashed contours in Figures 1A and 1B). As the T_1 of blood and tissue are slightly different at 9.4 T, contrast in T_1-weighted image may occur. However, after removal of the blood, the hyperintense layer was still evident in T_1-weighted images of the fixed brain (see white arrow in Figure 1C), although the fixation process slightly distorted the brain. In the histological image (Figure 1D), myelin clearly appeared as the dark band in the middle of the cortex, and Nissl substances (i.e., cell bodies) as black dots (see Figure 1E). As tissue shrinkage and distortion occur during fixation, the tissue slides were roughly coregistered to MR images, based on relative location to less-distorted white-matter structures. We observed a correlation between the myelin-rich dark stripe in the magnified histological image (Figure 1E) and the hyperintense band in the T_1-weighted image (from quadrangular box ROIs in Figure 1A), indicating that the hyperintensity within the cortex originated from myelin. These myelin-related profiles also agree with the profile of CBV_t-weighted images ($\Delta R^*_{2,\mathrm{MION}}$) (Figure 1F).

Dynamics and Magnitude of Functional Cerebral Blood Volume Changes

Visual stimulus-induced ΔCBV_a and relative CBV_t change maps were generated for the 40-second stimulation period (Figure 2). The greatest signal changes (yellow pixels in Figures 2B and 2C) in the cortex generally appeared in the area denoted by the

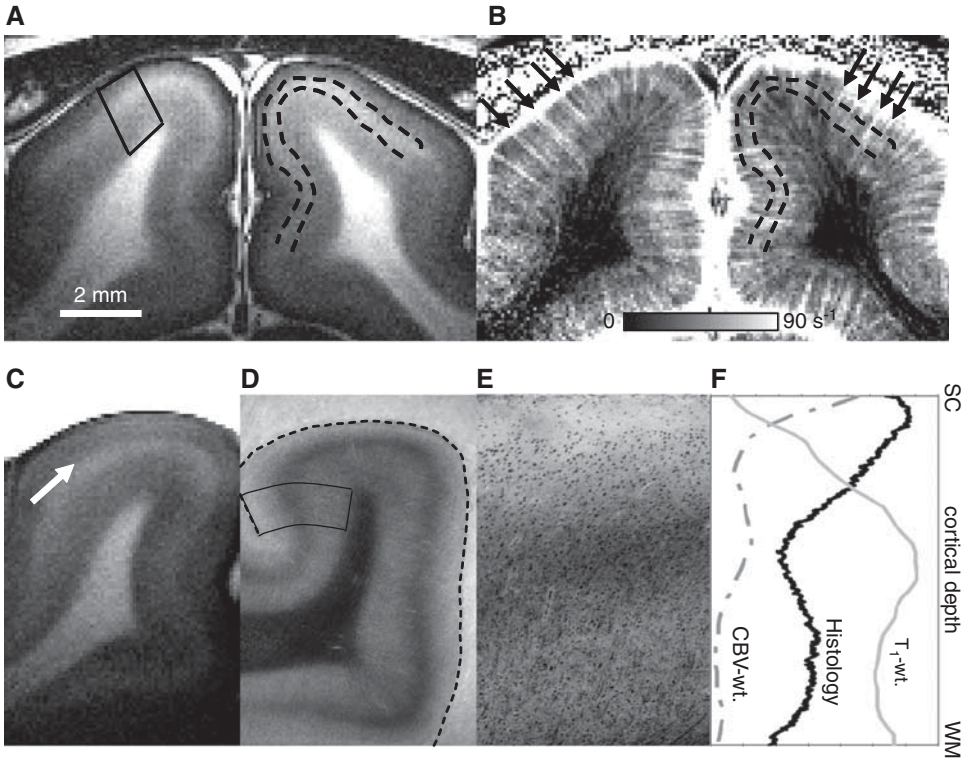

Figure 1 *In vivo* identification of the stripe of Gennari, layer 4 in the cat visual cortex. *In vivo* magnetic resonance (MR) images of one animal (**A**, **B**) were compared with fixed brain data of the same animal (**C**–**E**). (**A**) A coronal T_1-weighted image with inversion time (TI) = 1.4 seconds shows high intensity in middle cortical regions within gray matter (outlined by dashed lines) as well as white matter. Region of interest (ROI) was used for cortical profile analysis in (**F**). (**B**) Baseline total cerebral blood volume (CBV_t)-related $\Delta R2^*_{2,MION}$ map was calculated by MR signal changes induced by MION without stimulation. $\Delta R2^*_{2,MION}$ value (in gray bar) is linearly related to baseline CBV_t; CBV_t is the highest at the surface of the cortex, and the lowest in white matter. Arrows: penetrating intracortical vessels; dashed lines: identical as (**A**). (**C**) The hyperintense layer in the middle of the cortex (indicated by a white arrow) was still observed clearly in a T_1-weighted image of paraformaldehyde-fixed brain. (**D**–**E**) Histology was performed for myelin and Nissl staining. The myelin contrast was observed in white-matter tract, and as a dark band in the middle of the cortex, indicating layer 4. As the fixed tissue was shrunk and distorted by the histology process, the region corresponding to *in vivo* MR imaging ROI was selected. A magnified image of the ROI in (**D**) shows the myelin stain as dark horizontal band and Nissl substances as black dots (**E**). Dotted line: the cortical surface. (**F**) Cortical depth profile of magnified histological image is well correlated with that of T_1-weighted image and CBV_t-weighted map from the ROI in (**A**), especially in the middle of the cortex. MIONs, monocrystalline iron oxide nanoparticles; SC, surface of the cortex; WM, white matter.

two black dashed lines that represent the hyperintense stripes in T_1-weighted images (Figure 2A). This indicates that the greatest ΔCBV_a and ΔCBV_t happened within layer 4, consistent with our previous cortical layer-dependent fMRI studies (Kim and Kim, 2010; Zhao *et al*, 2006).

To determine the temporal dynamics, we obtained ΔCBV_a and $\Delta CBV_t/CBV_t$ time courses (Figure 3A) from the intracortical ROI (see yellow pixels in the inserted figure). Both *CBV* signals increased immediately following the stimulus onset, peaked within 10 seconds, and then slightly decreased during the remaining period of stimulation (Figure 3A). Assuming identical peak amplitudes for ΔCBV_t and ΔCBV_a (Kim *et al*, 2007), we calculated the baseline CBV_t value as 3.76 ± 1.34 mL/100 g tissue. We next converted $\Delta CBV_t/CBV_t$ time courses to ΔCBV_t time courses for the three baseline CBV_t values, for example, lower limit value, 4.5 and 5 mL/100 g (Figure 3B), and calculated the corresponding ΔCBV_v time courses (Figure 3C). Both ΔCBV_a and ΔCBV_t time courses showed rapid, positive changes after stimulus onset followed by small undershoots poststimulation (Figure 3B). In contrast, ΔCBV_v slowly increased after stimulus onset, and then slowly decreased without the poststimulus undershoots (Figure 3C). We observed significant CBV_v changes from baseline (see asterisk marks in Figure 3C) at 15 seconds after stimulation onset for a CBV_t of 3.76 mL/100 g (blue circles in Figure 3C). Although complex functions might fit the experimental data better, the simple single-exponential model captured the characteristics of arterial versus venous blood volume responses. Fitted functions of the averaged data were shown as solid lines in Figures 3B and 3C, and its results are summarized in Table 1. ΔCBV_a and ΔCBV_t responses with the lower baseline CBV_t limit yielded single-exponential time constants of

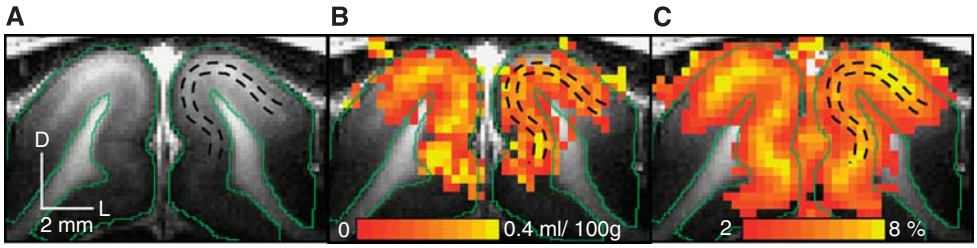

Figure 2 Relationship between anatomy (**A**) and functional cerebral blood volume (*CBV*) maps (**B**, **C**) of one animal. Stimulus-induced arterial *CBV* (ΔCBV_a) (**B**) and relative total *CBV* (CBV_t) change maps (**C**) show the highest *CBV* changes (yellow pixels) at layer 4, which is indentified by the hyperintense layer (between black dashed lines) in T_1-weighted image (**A**). D, dorsal; green contours, gray matter; L, left.

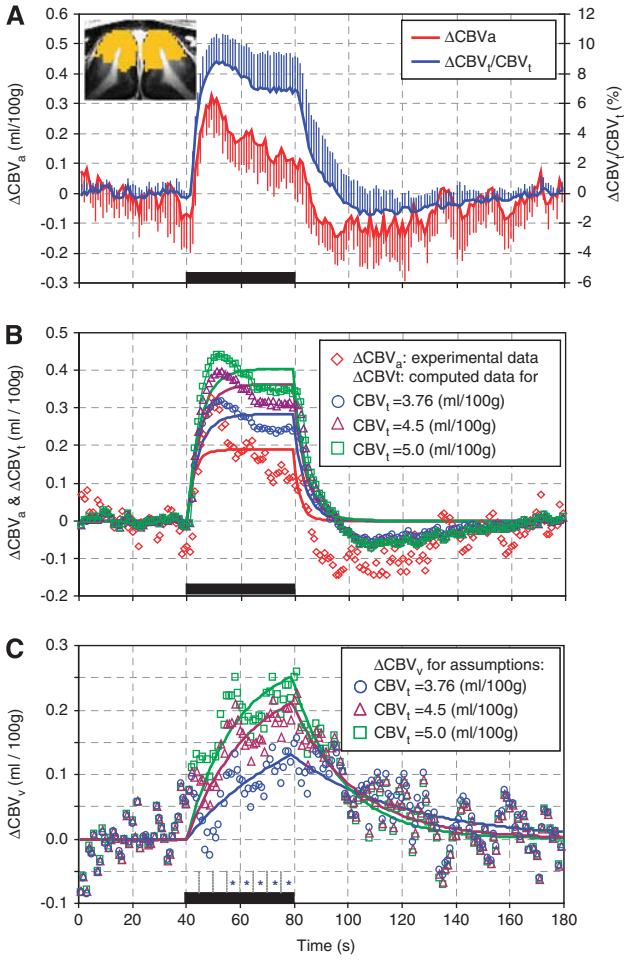

Figure 3 Dynamic functional changes of total, arterial, and venous cerebral blood volume (*CBV*). (**A**) Time courses of arterial *CBV* (ΔCBV_a) (red line) and total *CBV* (ΔCBV_t)/CBV_t (blue line) were obtained from the intracortical region of interest (ROI) (yellow pixels in inserted figure). Error bars: standard deviations ($n = 7$ animals). (**B**, **C**) To directly compare with ΔCBV_a (red diamonds), ΔCBV_t and ΔCBV_v were determined at three different baseline CBV_t conditions: the lower limit value ($= 3.76 \pm 1.34$ mL/100 g, $n = 7$) (blue circles), 4.5 mL/100 g (purple triangles), and 5.0 mL/100 g (green squares). Statistical significance of every 5-second ΔCBV_v activation data with the baseline CBV_t of 3.76 mL/100 g was calculated ($^*P < 0.05$). Average time courses were fit using a single-exponential function convoluted with a boxcar stimulation period. Best fits are plotted as colored solid lines (see also Table 1). Black bars indicates stimulation period.

2.68 ± 0.85 seconds and 4.93 ± 1.05 seconds and steady-state amplitudes of 0.19 ± 0.06 mL/100 g and 0.29 ± 0.06 mL/100 g, respectively. To examine region-dependent *CBV* responses, the intracortical ROI was divided into three cortical ROIs (Supplementary Figure S1); general temporal characteristics were consistent in all ROIs. When a higher baseline CBV_t was used, the amplitude of ΔCBV_t and ΔCBV_v increased, and the time constant of ΔCBV_v shortened. The time constant for ΔCBV_v is about an order of magnitude longer than that for ΔCBV_a (Table 1).

To investigate the stimulus-duration-dependent contribution of ΔCBV_v to ΔCBV_t, the ratio of mean ΔCBV_v to mean ΔCBV_t was calculated for the three baseline CBV_t conditions (Figure 4 for the intracortical ROI and Supplementary Figure S2 for the three cortical ROIs). As the peaks of ΔCBV_a and ΔCBV_t were assumed to be identical, and the time to reach 90% of the peak ΔCBV_a was 6.42 ± 2.58 seconds, initial 5 seconds data were not included for the $\Delta CBV_v/\Delta CBV_t$ calculations. Overall, the ratio of $\Delta CBV_v/\Delta CBV_t$ increased with stimulus duration, indicating that ΔCBV_v is significant during periods of long simulation.

Time-Dependent Spatial Specificity of Functional Cerebral Blood Volume Changes

To visualize the time-dependent fMRI maps, we divided the 40-second stimulation data into four equal time periods (Figure 5). During the initial 10-second period, ΔCBV_a and relative CBV_t change maps did not show a large volume change localized to layer 4, but during the later periods of stimulation, large changes did appear in this region (Figures 5A and 5B). This finding indicates delayed responses from small arterial vessels and presumably capillaries at the active site since the CBV_t response propagates from large arterial vessels to capillaries, and agrees with previous observations of ΔCBV_a (Kim and Kim, 2010) and relative CBV_t change (Jin and Kim, 2008*a*). Unlike ΔCBV_a and relative CBV_t change maps, ΔCBV_v was not localized to the middle cortical layer during the entire stimulation period (Figure 5C for the lower CBV_t limit and Supplementary Figure S3A for $CBV_t = 5.0$ mL/100 g). However, an

Table 1 Characteristics of functional CBV_a, CBV_t, and CBV_v responses

Baseline CBV_t *(mL/100 g)*	ΔCBV_a		ΔCBV_t		ΔCBV_v	
	Time constant (seconds)	*Amplitude (mL/100 g)*	*Time constant (seconds)*	*Amplitude (mL/100 g)*	*Time constant (seconds)*	*Amplitude (mL/100 g)*
3.76			4.29	0.28	40.87	0.13
4.5	2.53	0.18	4.71	0.36	23.36	0.21
5.0			4.71	0.40	18.36	0.25

Single-exponential time constant (seconds) and amplitude (mL blood/100 g tissue) were obtained by fitting the averaged time courses (Figures 3B and 3C) using a single-exponential function convoluted with a boxcar stimulus function. Three baseline CBV_t conditions were used.

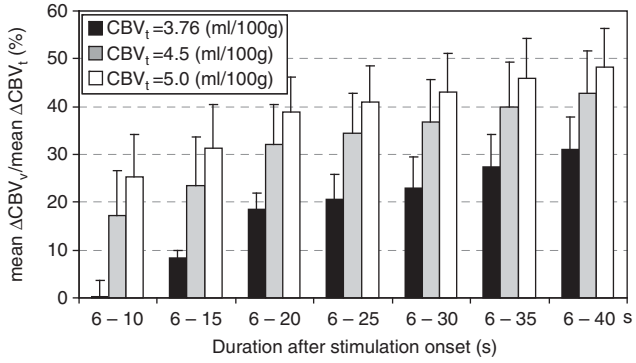

Figure 4 Stimulus-duration-dependent contribution of venous cerebral blood volume (*CBV*) to total *CBV* change ($n = 7$). The ratio of average ΔCBV_v to average total *CBV* (ΔCBV_t) increases was determined for different stimulus durations at three different baseline CBV_t values, 3.76 (black), 4.5 (gray), and 5.0 mL/100 g (white). Error bars: standard errors of means.

individual subject's ΔCBV_v map may not accurately reflect the spatial specificity and magnitude change due to the larger errors that result from pixel-wise subtraction (Figure 5C). Thus, group-averaged cortical depth profile analysis is necessary.

Cortical depth profiles were determined within the two black quadrangular ROIs shown in Figure 5A, and plotted as a function of depth from the cortical surface (Figure 6). The largest ΔCBV_a and relative CBV_t change during the 40-second stimulation period occurred in the middle cortical region (Figure 6A), which correlates with the hyperintensity band found in T_1-weighted anatomical images (Figure 1). For examining time-dependent spatial specificity, we plotted cortical depth profiles of ΔCBV_a (Figure 6B), ΔCBV_t (Figure 6C), and ΔCBV_v (Figure 6D). ΔCBV_t and ΔCBV_v profiles are shown for the lower limit value of baseline CBV_t (Figures 6C and 6D) and for a baseline CBV_t of 5 mL/100 g (Supplementary Figures S3B and S3C). Note that cortical profiles of ΔCBV during the poststimulus period were not plotted due to intersubject variations and insufficient signal-to-noise ratio. ΔCBV_a and ΔCBV_t profiles behaved similarly; both ΔCBV_a and ΔCBV_t were relatively large at the cortical surface during the initial 10-second period compared with later periods (blue lines). However, the greatest ΔCBV_a and ΔCBV_t responses for each time period occurred in the middle cortical region of later periods. In contrast, ΔCBV_v profiles were very broad across the cortex in all periods of stimulation (Figure 6D; Supplementary Figure S3C), indicating that the CBV_v change is not as specific as the CBV_a response. Note that the large ΔCBV_t and ΔCBV_v of the upper cortical area may have been due to the contribution of an extending susceptibility effect from pial vessels.

Discussion

Spatial Distribution of Functional Magnetic Resonance Imaging Versus Myeloarchitecture

In both arterial and total *CBV* fMRI studies, the highest *CBV* change within the cat's visual cortex occurred in layer 4, which was anatomically identified by T_1-weighted MRI (Figures 1 and 2). Similar studies using human and nonhuman primates also correlated the distinctive laminar myelination pattern of the cortex with fMRI results (Logothetis *et al*, 2002; Walters *et al*, 2003). This myeloarchitecture in the cortex has been identified in postmortem brain (Annese *et al*, 2004), and recently visualized by high-resolution MRI *in vivo* based on different imaging contrast, T_1 (Barbier *et al*, 2002; Bock *et al*, 2009; Walters *et al*, 2003), T_2 (Yoshiura *et al*, 2000), T_2^* (Logothetis *et al*, 2002), and proton density (Clark *et al*, 1992). In our studies, we used the T_1 contrast to identify the myelinated stripe of Gennari within the cortex, confirming the location of activation sites.

Technical Concerns of Cerebral Blood Volume Measurements

For ΔCBV_a quantification, we assumed that capillary water freely exchanges with tissue water; therefore, the venous contribution to MT-insensitive arterial blood measurement is negligible. Even if this assumption is not valid, the contribution of venous blood to ΔCBV_a will be minimal due to the very short T_2^* of venous blood at 9.4 T (Kim *et al*, 2008). We also assumed that the R_2^* of arterial blood ($R_{2,\text{artery}}^*$) and tissue ($R_{2,\text{tissue}}^*$) are similar, and that arterial oxygenation

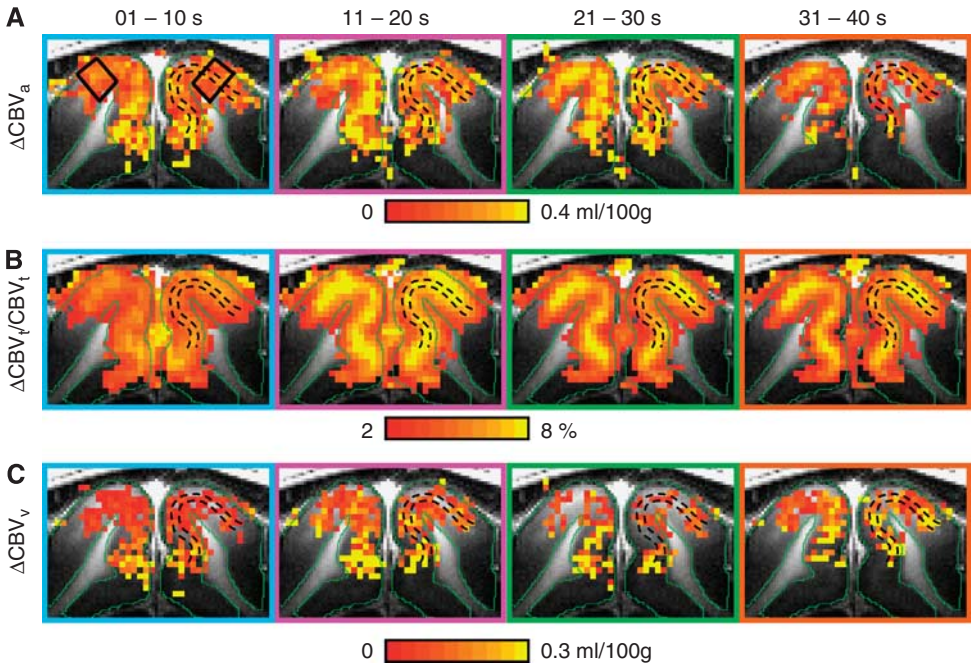

Figure 5 Time-dependent functional maps of total, arterial, and venous cerebral blood volume (*CBV*). Arterial *CBV* (ΔCBV_a) (**A**), total *CBV* (ΔCBV_t)/CBV_t (**B**), and ΔCBV_v (**C**) maps generated from one animal for 10-second period following stimulus onset. The ΔCBV_v maps were calculated from only positive active pixels in both ΔCBV_a and ΔCBV_t maps with baseline CBV_t of 3.66 (**C**) and 5 mL/100 g (Supplementary Figure S3A). It is noted that negative intercept pixels induced from the decrease in cerebrospinal fluid (CSF) volume fraction were not included in ΔCBV_a maps, and only pixels activated positively in both ΔCBV_a and ΔCBV_t maps were calculated for ΔCBV_v maps (see the area between the two hemispheres). Black dashed contours: hyperintense layer obtained from T_1-weighted image in the same animal; green contours: gray matter; two black regions of interest (ROIs): area 18 region for plotting cortical profiles in Figure 6.

does not change during stimulation (related to $\Delta R^*_{2,\text{artery}}$). However, the intravascular R_2^* of arterial blood has not been reported at 9.4 T, and a recent study showed a small increase in the oxygen saturation level in small pial arterial vessels during somatosensory stimulation in rats (Vazquez *et al*, 2010). Taking these two conditions into consideration, the intercept will be $\Delta v_a \times e^{-(R^*_{2,\text{artery}}+\Delta R^*_{2,\text{artery}}-R^*_{2,\text{tissue}})\times TE} + v_a \times e^{-(R^*_{2,\text{artery}}-R^*_{2,\text{tissue}})\times TE} \times (e^{-\Delta R^*_{2,\text{artery}}\times TE} - 1)$, where Δv_a is the change of arterial blood volume fraction (v_a). The measured intercept depends on $R^*_{2,\text{artery}}$ and $\Delta R^*_{2,\text{artery}}$ as well as Δv_a during stimulation. We evaluated Δv_a errors by computer simulation with various $R^*_{2,\text{artery}}$ and $\Delta R^*_{2,\text{artery}}$ values (Supplementary Figure S4). Δv_a might have significant error, but this will not affect to the dynamic property and spatial localization of arterial and venous CBV changes. Thus, our findings are not changed.

In pixels containing CSF, both arterial blood and CSF are MT insensitive; thus, the interpretation of intercepts from $\Delta S_{ss,MT}/S_0$ versus $S_{ss,MT}/S_0$ fit is complex if the CSF volume fraction changes during stimulation. We found that CSF volume fraction decreases in cats during similar visual stimulation (Jin and Kim, 2010), resulting in negative responses in ΔCBV_a maps (Kim and Kim, 2010). Thus, ΔCBV_a values were only determined when intercepts were positive and ΔCBV_v maps were consequently calculated from only those pixels (Figure 5C). When the intracortical ROI with 173 ± 54 pixels (see yellow area in inserted figure of Figure 3A) was considered, the number of negative pixels was 25 ± 10. These negative pixels were primarily found at the cortical surface, and thus ΔCBV_a and ΔCBV_v profiles near that region may have larger errors.

ΔCBV_t and ΔCBV_v were obtained within a range of baseline CBV_t values. As CBV_t of gray matter is 2 to 5 mL/100 g in the literature (Ibaraki *et al*, 2008; Kuppusamy *et al*, 1996; Sourbron *et al*, 2009), our upper limit of baseline CBV_t was set to 5 mL/100 g. As $\Delta CBV_a \leqslant \Delta CBV_t$ at any time, the lower baseline limit for CBV_t (3.76 ± 1.34 mL/100 g) was calculated by assuming that peak ΔCBV_t = peak ΔCBV_a. In fact, ΔCBV_a is dominant during the 15-second stimulation (Kim *et al*, 2007) and arterial vessel dilation (but not venous dilation) was observed by optical imaging of intrinsic signals with a 20-second stimulation (Vazquez *et al*). When peak ΔCBV_t matched with peak ΔCBV_a for each ROI, the baseline CBV_t was 4.04 ± 1.67, 3.70 ± 1.61, and 3.68 ± 1.66 mL/100 g for the upper, middle, and lower cortical ROI, respectively. The average $\Delta R^*_{2,\text{MION}}$ value, which is an index of baseline CBV_t, was 41.70 ± 20.01, 35.55 ± 17.97, and 28.51 ± 15.88/s for upper, middle, and lower cortical ROI, respectively. Although large standard deviations are due to the different dose of injected

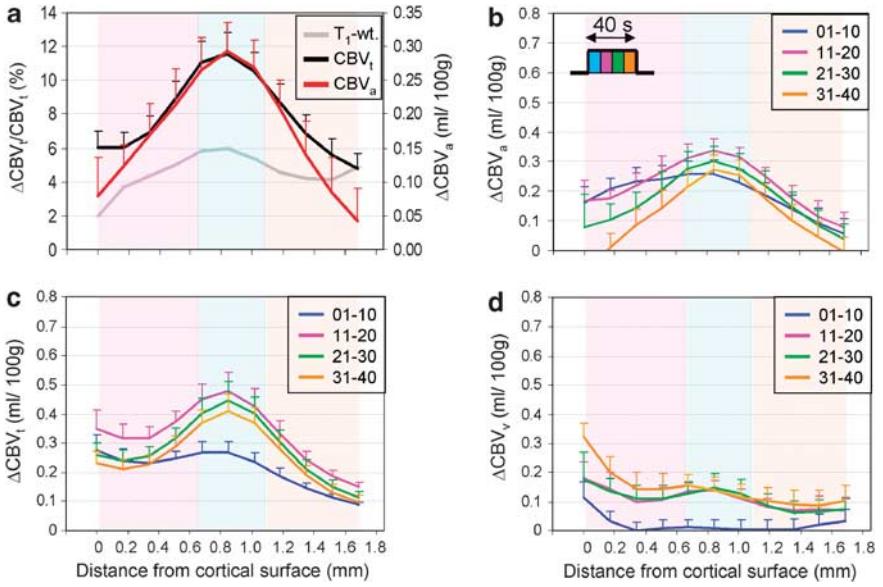

Figure 6 Cortical profiles in visual cortical area 18 ($n = 7$). Cortical depth profiles were generated from the regions of interest (ROIs) (black quadrangular ROIs in Figure 5A) in each animal. (**A**) Average profiles of arterial *CBV* (ΔCBV_a) and total *CBV* (ΔCBV_t) obtained for the entire 40-second stimulation period correlate well with that of T_1-weighted image. T_1-weighted profile ranged between 4.3 and 7.0 (arbitrary unit) is plotted with the adjusted scale for better visualization. (**B**–**D**) Average cortical depth profiles ($n = 7$) of ΔCBV_a (**B**), ΔCBV_t (**C**), and ΔCBV_v (**D**) were calculated at every 10-second time period. ΔCBV_t and ΔCBV_v profiles were calculated with baseline CBV_t of 3.76 (**C**, **D**) and 5 mL/100 g (Supplementary Figures S3B and S3C). Both ΔCBV_a and ΔCBV_t responses are relatively high at the cortical surface initially, and the highest at layer 4 at > 10 seconds after stimulation onset (**B**, **C**), while ΔCBV_v has very little laminar specificity (**D**). Error bars: standard errors of means; color bands: upper (layers 2 to 3), middle (layer 4), and lower (layers 5 to 6) cortical layers. CBV, cerebral blood volume.

MION between animals, baseline CBV_t correlates well with $\Delta R^*_{2,\mathrm{MION}}$. Taken together, the assumption of peak ΔCBV_t = peak ΔCBV_a appears reasonable.

Dynamics of Functional CBV_a and CBV_v Responses

The dynamic characteristics of the CBV_t response has been previously described in the literature as two components: an early rapid rise followed by a prolonged slower response (Mandeville *et al*, 1999; Silva *et al*, 2007). Yet, the origin of these two components remains unclear. Mandeville *et al* (1999) proposed that the rapid capillary response is followed by the late slow venous vessel dilation, which is referred to as the 'Windkessel model'. However, Silva *et al* (2007) assumed that, based on the gamma fit of the CBV_t, the fast rise and fall response originates from arteries, while the slow and delayed response originates from capillaries. Our data imply that fast and slow *CBV* responses stem from an initial rapid arterial vasodilation followed by slow prolonged venous dilation. Increased venous volume is likely due to passive dilation of high compliance venous vessels, resulting from the increased pressure associated with arteriole vasodilation (Buxton *et al*, 1998; Mandeville *et al*, 1999). In our studies, capillary volume change cannot be separately determined, and will contribute to ΔCBV_a and ΔCBV_v. As capillary dilation is expected to be specific to neural active sites, and ΔCBV_v is not specific, capillary dilation, if present, will contribute mostly to ΔCBV_a.

As the functional CBV_v response is an order of magnitude slower than CBV_a change, the contribution of ΔCBV_v to ΔCBV_t is closely dependent on stimulus duration (Figure 4). A similar dynamic dilation of arterial versus venous vessels was also detected by two-photon microscopic measurements during somatosensory stimulation in awake mice (Patrick Drew, personal communication). Venous vessels dilate passively and slowly; thus, its response time constant is much longer than the expected time constant, which is a sum of the arterial response time and the arterial–venous transit time of 1 to 2 seconds. Under steady-state conditions, ΔCBV_v is about half of ΔCBV_t (see Table 1). When the stimulus duration is relatively short compared with the ΔCBV_v time constant, the CBV_a change is dominant. Temporal characteristics of arterial and venous *CBV* responses may vary under different cerebrovascular conditions (e.g., due to different anesthetics or baseline arterial CO_2 level); thus, extrapolation of our data to different anesthetic conditions or awake humans requires a degree of caution. In our previous 15-second stimulation studies in isoflurane-anesthetized rats, we found that CBV_a is dominant (Kim *et al*, 2007). Dilation

of arterial, not venous vessels was observed using two-photon microscopic studies with 4 seconds somatosensory stimulation in α-chloralose-anesthetized rats (Hillman *et al*, 2007) and optical imaging of intrinsic signals with 20 seconds stimulation in isoflurane-anesthetized rats (Vazquez *et al*). Our finding may explain the substantial ΔCBV_v increase with 96 to 240 seconds long visual stimulation in humans (Chen and Pike, 2009; Stefanovic and Pike, 2005), and venous dilation during the 120-second long direct electric stimulation in halothane-anesthetized rats (Akgoren and Lauritzen, 1999).

Spatial Specificity of Functional CBV_a and CBV_v Responses

To have high specificity of *CBV* responses to neural active sites, it is crucial to detect the dilation of microvessels, including capillaries. The CBV_t response across the visual cortex localizes to the middle of the cortex, where the highest neural activity, as well as metabolic and cerebral blood flow (*CBF*) changes occur (Jin and Kim, 2008*a*; Zhao *et al*, 2006). However, as both fast ΔCBV_a and slow ΔCBV_v contribute to ΔCBV_t, time-dependent spatial specificity of arterial and venous *CBV* responses can provide insights into further sources of functional *CBV* changes. During the initial 10 seconds of stimulation, both CBV_a and CBV_t responses are relatively large at the upper cortical area, indicating the dilation of intracortical feeding arterial macrovessels. Between 10 and 20 seconds after stimulation onset, CBV_a and CBV_t responses at the middle of the cortex increase, possibly due to further dilation of arterial microvessels. Our high specificity finding can be interpreted that increases of arterial microvessels dominate and improve spatial specificity for CBV_t fMRI. Thus, the stimulus period of 10 to 20 seconds induces the dilation of arterial microvessels without significant contribution from venous vessels, resulting in spatially confined CBV_t responses. A similar observation was found with optical imaging (Berwick *et al*, 2008); the *CBV* response was initially dominated by feeding arteries, and then highly localized to a central area of the activated cortical column, albeit at a much faster time scale, possibly due to different vascular structures in different activated areas (rat barrels versus cat visual cortex) and different neurovascular responses from different anesthesia conditions (urethane versus isoflurane).

Draining venules are connected to highly specific, actively controlled arterioles through capillaries. As passive pressure-driven dilation should start at venous microvessels, we expected ΔCBV_v to be specific. The contribution of CSF and pial vessels can cause errors in ΔCBV_a and ΔCBV_v quantification for the upper cortical area, but not for the middle and lower cortical areas. The spatial specificity of ΔCBV_v (see middle versus lower cortical area in Figure 6) is relatively poor compared with ΔCBV_a and ΔCBV_t. The localization of ΔCBV_v may improve with a longer stimulus or more averaging, since 40 seconds duration may not be sufficiently long to reach to steady state and the noise of ΔCBV_v is higher than that of ΔCBV_a. The firm conclusion of spatial specificity may require a direct measurement of ΔCBV_v. To explain the difference of spatial specificity between arterial and venous microvessel responses, determining the number and length of venous vessels drained from a single arteriole is also necessary.

Implication for Blood Oxygenation Level-Dependent Quantification

Relative (rather than absolute) CBV_v change is important to determine the change in cerebral metabolic rate of oxygen consumption ($CMRO_2$) from BOLD data. Conventionally, it is assumed that the relative CBV_v ($rCBV_v$) change is equal to the relative CBV_t ($rCBV_t$) change, which is determined from the measured relative *CBF* (*rCBF*) change using the Grubb's *CBF*–*CBV* relationship, $rCBV_t = rCBF^{\alpha}$, where α is considered to be 0.38 (Grubb *et al*, 1974). To calibrate BOLD signals with physiological parameters, BOLD and *CBF* responses are measured during a hypercapnic challenge, assuming no $CMRO_2$ change. A fundamental assumption of hypercapnic calibration is that hemodynamic changes during hypercapnia and neural stimulation are similar. In our studies, the venous *CBV* response is relatively slow and sensitive to stimulus duration. In long stimulation studies, typically implemented for a hypercapnic challenge (more than a few minutes (Davis *et al*, 1998; Hoge *et al*, 1999; Kim *et al*, 1999)), ΔCBV_v is ~50% of ΔCBV_t (see Table 1). In our laboratory's previous CBV_a and CBV_v measurements with ^{19}F nuclear magnetic resonance (NMR) spectroscopy, ΔCBV_v contributes ~36% to ΔCBV_t with hypercapnia (Lee *et al*, 2001), which is similar to our current visual stimulation data. To convert ΔCBV_v to the $rCBV_v$ change, baseline CBV_v is required. In the following estimates, we assume that baseline CBV_t of 3.76 mL/100 g consists of 25% to 40% CBV_a and 75% to 60% CBV_v (Kim *et al*, 2007; Lee *et al*, 2001). When ΔCBV_v is 36% to 50% of ΔCBV_t under steady-state conditions, $rCBV_v$ change is ~50% to 60% to ~70% to 80% of $rCBV_t$ change. For neural stimulation, stimulus duration is typically in the order of seconds to tens of seconds. In our 40-second visual stimulation studies, ΔCBV_v is 31% of ΔCBV_t, consequently $rCBV_v$ is ~40% to 50% of $rCBV_t$. However, if the stimulation duration is < 20 seconds, $rCBV_v$ is much smaller and could be even ignored. Thus, short stimulation simplifies the BOLD biophysical model, but a long neural stimulation would be better to match corresponding cerebrovascular responses with a long hypercapnic challenge for the calculation of $CMRO_2$.

The BOLD signal is closely dependent on the alterations in venous oxygenation level (*Y*)

and venous *CBV* (CBV_v), and can be linearly approximated as

$$\Delta R_2^* = \alpha \times (1-Y) \times CBV_v \{\Delta Y/(1-Y) - (\Delta CBV_v/CBV_v)\}$$
$$= M\{1 - (\Delta CMRO_2/CMRO_2 + 1)/(\Delta CBF/CBF + 1) - (\Delta CBV_v/CBV_v)\}$$

where ΔR_2^* is the change in apparent transverse relaxation rate, M is $\alpha \times (1-Y) \times CBV_v$ (same as α^* in Kim *et al* (1999)), and Δ indicates a change in physiological parameter; the parameter α is closely related to many biological and MR parameters, including vessel size, magnetic field, and pulse sequence. It is also noted that the term $\beta^* = 1$ (Kim *et al*, 1999). To determine the effect of slow CBV_v change to $CMRO_2$ quantification, we calculated relative $CMRO_2$ changes with three CBV_v response conditions from the human visual cortex data reported in Kim *et al* (1999), which are $\Delta CBF/CBF$ and ΔR_2^* of 47% and −0.45/s during 4 minutes hypercapnia, and 44% and −0.11/s during 1 minute visual stimulation, respectively. In all conditions, the $rCBV_t$ change can be calculated from $\Delta CBF/CBF$ using the Grubb's equation: (1) When it is assumed that the $rCBV_v$ change = the $rCBV_t$ change, which has been widely used in the fMRI community, the relative $CMRO_2$ change is 17%. (2) If the $rCBV_v$ change is half of the $rCBV_t$ change in both hypercapnia and visual stimulation, then the relative $CMRO_2$ change is 25%. (3) If the $rCBV_v$ change is half of the $rCBV_t$ change in hypercapnia and close to zero in visual stimulation, then the relative $CMRO_2$ change is 36%. The ratio of relative $CMRO_2$ to *CBF* change is 0.39, 0.57, and 0.82, depending on the different *rCBF* versus $rCBV_v$ conditions. The proper estimation of $rCBV_v$ changes is important to quantify relative $CMRO_2$ and venous oxygenation level changes from BOLD signals.

Acknowledgements

The authors thank Dr Ping Wang for animal preparation and maintenance during the experiments. We thank Dr Patrick J Drew for helpful discussions and for sharing unpublished data.

Disclosure/conflict of interest

The authors declare no conflict of interest.

References

Akgoren N, Lauritzen M (1999) Functional recruitment of red blood cells to rat brain microcirculation accompanying increased neuronal activity in cerebellar cortex. *Neuroreport* 10:3257–63

Annese J, Pitiot A, Dinov ID, Toga AW (2004) A myeloarchitectonic method for the structural classification of cortical areas. *Neuroimage* 21:15–26

Barbier EL, Marrett S, Danek A, Vortmeyer A, van Gelderen P, Duyn J, Bandettini P, Grafman J, Koretsky AP (2002) Imaging cortical anatomy by high-resolution MR at 3.0T: detection of the stripe of Gennari in visual area 17. *Magn Reson Med* 48:735–8

Berwick J, Johnston D, Jones M, Martindale J, Martin C, Kennerley AJ, Redgrave P, Mayhew JE (2008) Fine detail of neurovascular coupling revealed by spatiotemporal analysis of the hemodynamic response to single whisker stimulation in rat barrel cortex. *J Neurophysiol* 99:787–98

Bock NA, Kocharyan A, Liu JV, Silva AC (2009) Visualizing the entire cortical myelination pattern in marmosets with magnetic resonance imaging. *J Neurosci Methods* 185:15–22

Buxton RB, Wong EC, Frank LR (1998) Dynamics of blood flow and oxygenation changes during brain activation: the balloon model. *Magn Reson Med* 39:855–64

Chen JJ, Pike GB (2009) BOLD-specific cerebral blood volume and blood flow changes during neuronal activation in humans. *NMR Biomed* 22:1054–62

Clark VP, Courchesne E, Grafe M (1992) *In vivo* myeloarchitectonic analysis of human striate and extrastriate cortex using magnetic resonance imaging. *Cereb Cortex* 2:417–24

Davis TL, Kwong KK, Weisskoff RM, Rosen BR (1998) Calibrated functional MRI: mapping the dynamics of oxidative metabolism. *Proc Natl Acad Sci USA* 95:1834–9

Goense JB, Logothetis NK (2006) Laminar specificity in monkey V1 using high-resolution SE-fMRI. *Magn Reson Imaging* 24:381–92

Grubb RL, Jr, Raichle ME, Eichling JO, Ter-Pogossian MM (1974) The effects of changes in PaCO2 on cerebral blood volume, blood flow, and vascular mean transit time. *Stroke* 5:630–9

Harel N, Lin J, Moeller S, Ugurbil K, Yacoub E (2006) Combined imaging-histological study of cortical laminar specificity of fMRI signals. *Neuroimage* 29:879–87

Herscovitch P, Raichle ME (1985) What is the correct value for the brain—blood partition coefficient for water? *J Cereb Blood Flow Metab* 5:65–9

Hillman EM, Devor A, Bouchard MB, Dunn AK, Krauss GW, Skoch J, Bacskai BJ, Dale AM, Boas DA (2007) Depth-resolved optical imaging and microscopy of vascular compartment dynamics during somatosensory stimulation. *Neuroimage* 35:89–104

Hoge RD, Atkinson J, Gill B, Crelier GR, Marrett S, Pike GB (1999) Investigation of BOLD signal dependence on cerebral blood flow and oxygen consumption: the deoxyhemoglobin dilution model. *Magn Reson Med* 42:849–63

Ibaraki M, Miura S, Shimosegawa E, Sugawara S, Mizuta T, Ishikawa A, Amano M (2008) Quantification of cerebral blood flow and oxygen metabolism with 3-dimensional PET and 15O: validation by comparison with 2-dimensional PET. *J Nucl Med* 49:50–9

Jin T, Kim SG (2008*a*) Cortical layer-dependent dynamic blood oxygenation, cerebral blood flow and cerebral blood volume responses during visual stimulation. *Neuroimage* 43:1–9

Jin T, Kim SG (2008*b*) Improved cortical-layer specificity of vascular space occupancy fMRI with slab inversion relative to spin-echo BOLD at 9.4 T. *Neuroimage* 40: 59–67

Jin T, Kim SG (2010) Change of the cerebrospinal fluid volume during brain activation investigated by T(1rho)-weighted fMRI. *Neuroimage* 51:1378–83

Kennan RP, Scanley BE, Innis RB, Gore JC (1998) Physiological basis for BOLD MR signal changes due to neuronal stimulation: separation of blood volume and magnetic susceptibility effects. *Magn Reson Med* 40:840–6

Kim SG, Rostrup E, Larsson HB, Ogawa S, Paulson OB (1999) Determination of relative $CMRO_2$ from CBF and BOLD changes: significant increase of oxygen consumption rate during visual stimulation. *Magn Reson Med* 41:1152–61

Kim T, Hendrich K, Kim SG (2008) Functional MRI with magnetization transfer effects: determination of BOLD and arterial blood volume changes. *Magn Reson Med* 60:1518–23

Kim T, Hendrich KS, Masamoto K, Kim SG (2007) Arterial versus total blood volume changes during neural activity-induced cerebral blood flow change: implication for BOLD fMRI. *J Cereb Blood Flow Metab* 27: 1235–47

Kim T, Kim SG (2010) Cortical layer-dependent arterial blood volume changes: improved spatial specificity relative to BOLD fMRI. *Neuroimage* 49:1340–9

Kuppusamy K, Lin W, Cizek GR, Haacke EM (1996) *In vivo* regional cerebral blood volume: quantitative assessment with 3D T1-weighted pre- and postcontrast MR imaging. *Radiology* 201:106–12

Lee SP, Duong TQ, Yang G, Iadecola C, Kim SG (2001) Relative changes of cerebral arterial and venous blood volumes during increased cerebral blood flow: implications for BOLD fMRI. *Magn Reson Med* 45:791–800

Logothetis N, Merkle H, Augath M, Trinath T, Ugurbil K (2002) Ultra high-resolution fMRI in monkeys with implanted RF coils. *Neuron* 35:227–42

Lu H, Patel S, Luo F, Li SJ, Hillard CJ, Ward BD, Hyde JS (2004) Spatial correlations of laminar BOLD and CBV responses to rat whisker stimulation with neuronal activity localized by Fos expression. *Magn Reson Med* 52:1060–8

Mandeville JB, Marota JJ (1999) Vascular filters of functional MRI: spatial localization using BOLD and CBV contrast. *Magn Reson Med* 42:591–8

Mandeville JB, Marota JJA, Ayata C, Zaharchuk G, Moskowitz MA, Rosen B, Weisskoff R (1999) Evidence of a cerebrovascular postarteriole windkessel with delayed compliance. *J Cereb Blood Flow Metab* 19:679–89

Payne BR, Peters A (2002) The concept of cat primary visual cortex. In: *The Cat Primary Visual Cortex* (Payne BR, Peters A, eds), Academic Press: San Diego, London, Boston, New York, Sydney, Tokyo, Toronto, pp 1–129

Silva AC, Koretsky AP, Duyn JH (2007) Functional MRI impulse response for BOLD and CBV contrast in rat somatosensory cortex. *Magn Reson Med* 57:1110–8

Sourbron S, Ingrisch M, Siefert A, Reiser M, Herrmann K (2009) Quantification of cerebral blood flow, cerebral blood volume, and blood-brain-barrier leakage with DCE-MRI. *Magn Reson Med* 62:205–17

Stefanovic B, Pike GB (2005) Venous refocusing for volume estimation: VERVE functional magnetic resonance imaging. *Magn Reson Med* 53:339–47

Tieman SB, Mollers S, Tieman DG, White J (2004) The blood supply of the cat's visual cortex and its postnatal development. *Brain Res* 998:100–12

Vazquez AL, Fukuda M, Tasker ML, Masamoto K, Kim SG (2010) Changes in cerebral arterial, tissue and venous oxygenation with evoked neural stimulation: implications for hemoglobin-based functional neuroimaging. *J Cereb Blood Flow Metab* 30:428–39

Walters NB, Egan GF, Kril JJ, Kean M, Waley P, Jenkinson M, Watson JD (2003) *In vivo* identification of human cortical areas using high-resolution MRI: an approach to cerebral structure-function correlation. *Proc Natl Acad Sci USA* 100:2981–6

Woolsey TA, Rovainen CM, Cox SB, Henegar MH, Liang GE, Liu D, Moskalenko YE, Sui J, Wei L (1996) Neuronal units linked to microvascular modules in cerebral cortex: response elements for imaging the brain. *Cereb Cortex* 6:647–60

Yoshiura T, Higano S, Rubio A, Shrier DA, Kwok WE, Iwanaga S, Numaguchi Y (2000) Heschl and superior temporal gyri: low signal intensity of the cortex on T2-weighted MR images of the normal brain. *Radiology* 214:217–21

Zhao F, Wang P, Hendrich KS, Ugurbil K, Kim SG (2006) Cortical layer-dependent BOLD and CBV responses measured by spin-echo and gradient-echo fMRI: insights into hemodynamic regulation. *NeuroImage* 30:1149–60

Supplementary Information accompanies the paper on the Journal of Cerebral Blood Flow & Metabolism website (http://www.nature.com/jcbfm)